ORIGINAL RESEARCH

# Carbon Nanospheres Exert Antitumor Effects Associated with Downregulation of 4E-BP1 Expression on Prostate Cancer

Weimin Dong[1]
Yong Luo[2]
Guian Zhang[1]
Hui Zhang[1]
Yuxiang Liang[1]
Yangjia Zhuo[1]
Yingke Liang[1]
Fen Zou[1]
Weide Zhong [1,3,4]

[1]Department of Urology, Guangdong Key Laboratory of Clinical Molecular Medicine and Diagnostics, Guangzhou First People's Hospital, School of Medicine, South China University of Technology, Guangzhou, Guangdong 510180, People's Republic of China; [2]Department of Urology, The Second People's Hospital of Foshan, Affiliated Foshan Hospital of Southern Medical University, Foshan 528000, People's Republic of China; [3]Department of Urology, Huadu District People's Hospital, Southern Medical University, Guangzhou 510800, People's Republic of China; [4]Urology Key Laboratory of Guangdong Province, The First Affiliated Hospital of Guangzhou Medical University, Guangzhou Medical University, Guangzhou 510230, People's Republic of China

Correspondence: Weide Zhong; Fen Zou
Department of Urology, Guangdong Key Laboratory of Clinical Molecular Medicine and Diagnostics, Guangzhou First People's Hospital, School of Medicine, South China University of Technology, Guangzhou 510180, People's Republic of China
Tel +86 20-81048312
Fax +86 20-8337332
Email zhongwd2009@live.cn;
zoufen2008@126.com

**Introduction:** Although carbon nanospheres (CNPs) are promising nanomaterials in cancer treatment, how they affect prostate cancer (PCa) remains unclear.

**Methods:** In this study, scanning electron microscopy (SEM), X-ray diffraction (XRD), and Raman spectroscopy were used to confirm the successful synthesis of CNPs. CCK-8, flow cytometry, Transwell, wound healing, Western blot and immunohistochemistry (IHC) assays were performed to evaluate the antitumor effect of CNPs toward the two kinds of prostate cancer cell lines PC3 and DU145.

**Results:** Our results showed that CNPs inhibited cell growth, invasion, and migration and induced apoptosis and autophagy in PCa cells. Multifactor detection of a single *Akt* phosphorylation pathway and Western blot results suggested the suppression of *4E-BP1* in PCa cells after incubation with CNPs. The results from animal experiments also suggested the antitumor effect of CNPs and reduced *4E-BP1* expression in PCa tissue samples from *BALB/c nude mice* administered a local subcutaneous injection of CNPs.

**Keywords:** carbon nanosphere, prostate cancer, antitumor, *4E-BP1*

## Introduction

Prostate cancer (PCa) is one of the most common cancers in males and is known for its high incidence and mortality.[1] Considering that the 5-year survival rate is up to 98%,[1] the early diagnosis and treatment of PCa are particularly essential. The current therapy for localized PCa is radical prostatectomy.[2] However, this treatment is not satisfactory considering the development of side effects, such as urinary incontinence and erectile dysfunction.[3] If the PCa has spread, radiation therapy, chemotherapy, or hormone therapy are used before surgery. Nevertheless, discomfort caused by these treatments includes pain, weakness, and nervous system disorder that cannot be ignored. Instead, the development of nanomaterials, molecular diagnosis and precise treatments, including nanomedicine, are approaches that now play a relatively critical crucial role in cancer therapy.[4] Thus, understanding how nanomaterials affect prostate cancer is urgently needed.

Nanomaterials have been widely used as drug and gene delivery agents in tumor research in the past few years.[5,6] Several studies have indicated that delivery systems based on nanomaterials suppress tumor growth in vivo.[7–9] The first carbon nanomaterial was developed in the 1970s.[10] Unlike studies on other nanocarbon particles, such as carbon nanotubes (CNTs),[11–13] research on carbon nanospheres (CNPs) is limited.[14] Because CNPs are easily internalized into cells with excellent biocompatibility, they

can be used for drug, gene, and protein delivery.[15] CNPs were reported to inhibit the growth of PCa by promoting maximal energy transfer in microwave therapy without strong biotoxicity in a long-term animal study.[16] Nanocarbon appears to be a promising cancer therapy material for the future. However, the mechanism by which CNPs themselves affect tumors is not completely understood. Thus, the goal of the investigation was to study how CNPs affect PCa in vivo and in vitro.

# Materials and Methods
## Synthesis of CNPs
CNPs were prepared by the glucose hydrothermal method[17] and characterized by scanning electron microscopy (SEM) and X-ray diffraction (XRD). A Raman spectrometer was used to verify the structural composition. In brief, a glucose solution was heated to 400°C for 4 h and then filtered after cooling to room temperature.

## Culturing of Cell Lines
DU145 and PC3 are two commonly used PCa cell lines, while BPH-1 is a benign prostate epithelial cell line. Cell lines were purchased from the American Type Culture Collection (ATCC) (Manassas, VA, USA) and authenticated by HYY Med company (Guangzhou, China). The PCa and prostate epithelial cells were cultured separately in DMEM (HyClone, Logan, UT, USA) or RPMI-1640 medium (Cellgro, Manassas, VA, USA) supplemented with 10% fetal bovine serum (Gibco, Grand Island, NY, USA) and 1% penicillin/streptomycin under an atmosphere with 5% $CO_2$ at 37°C.

## Cell Cycle Analysis
According to the protocol of our previous research,[18] cells treated or not treated with medium containing 10 μg/mL CNPs were collected, washed twice with PBS, and fixed overnight in 70% ethanol at 4°C. A staining buffer containing 500 μL of PBS, propidium iodide (PI; 5 μg/mL), RNaseA (100 μg/mL), and 0.3 μL of 0.3% Triton X-100 was added to the cells, which were then incubated at 4 °C for 30 min. Subsequently, a flow cytometer (BD FACSVerse, BD Biosciences, USA) and FlowJo were used to analyze the cells and results. Three independent experiments were performed and repeated at least three times.

## Apoptosis Detection
DU145 and PC3 cells were prestimulated with CNPs (CNPs group) or left unstimulated (control group) for

24 h. Then, the cells were harvested by trypsinization and incubated with 5 μL of Annexin V-APC and 10 μL of 7AAD. After the cells were vortexed and incubated at room temperature in the dark for 15 min, 485 μL of 1× binding buffer was added to each tube. A flow cytometer (BD FACSVerse, BD Biosciences, USA) were used to analyze the results. Three independent experiments were performed and repeated at least three times.

## Cell Proliferation Assay
DU145 and PC3 cells were seeded in 96-well plates. After 24 h, the medium was changed to medium containing 5 or 10 μg/mL CNPs. After another 24, 48, or 72 h, a 10% CCK-8 (C0038, Beyotime, China) solution was added to each well. The absorbance at 450 nm was measured on a spectrophotometer (Multiskan MK3, Thermo Scientific). Three independent experiments were performed and repeated at least three times.

## Cell Invasion Assay
Transwell assays were used to determine cell invasion. 20 μ Matrigel (BD Biosciences) diluted 8-fold with serum-free medium was coated into the upper Transwell chamber, which was then placed in 24-well plate. A total of $5 \times 10^4$ DU145 or PC3 cells treated with medium containing 10 μg/mL of CNPs or left untreated for 24 h were seeded in the upper compartment of the chamber. Then, 500 μL of complete culture medium was added to the lower compartment. After incubating at 37°C under an atmosphere with 5% $CO_2$ for 24 or 48 h, the cells remaining in the upper chamber were removed, and the remaining cells were fixed with methanol for 20 min and stained with 0.1% crystal violet for 10–20 min. Transwell assay results were quantified by using Image-Pro Plus. Three independent experiments were performed and repeated at least three times.

## Cell Migration Assay
Wound-healing assays were performed to evaluate cell migration. DU145 and PC3 cells were seeded in 6-well plates and incubated until they reached 80% confluence. After scratches were made in the cell layers with sterile pipette tips, the cells were washed with PBS three times. Then, complete culture medium containing mitomycin was added. Microscopic observations were performed at 24 and 30 h after scratching. Three independent experiments were performed and repeated at least three times.

## Western Blot Analysis

DU145 and PC3 cells were stimulated with 10 μg/mL CNPs for 24 h and then lysed in RIPA lysis buffer containing 1% PMSF and phosphatase inhibitors. Then, 10–25 μg of lysate proteins were separated by 10 or 12% SDS-PAGE and transferred to PVDF membranes (#ISEQ00010, Millipore). The membranes were blocked with 5% skim milk (#232100, BD Difco) in TBST at room temperature for 1 h and then incubated with anti-*Caspase-3* (#9662, Cell Signaling Technology), anti-*Cleaved Caspase-3* (#9664S, Cell Signaling Technology), anti-LC3 (NB100-2331, Novus Biologicals), anti-*SQSTM1* (sc-48402, Santa Cruz), anti-*4E-BP1* (#9452, Cell Signaling Technology), anti-*Vimentin* (#5741T, Cell Signaling Technology), anti-*E-Cadherin* (#3195T, Cell Signaling Technology), and Anti-β-actin antibodies (BM0627, Boster Biological Technology) at 4°C overnight. Subsequently, the membranes were incubated with an appropriate secondary antibody at room temperature for 1 h. Immobilon Western chemiluminescent HRP substrate was used to visualize the resulting protein bands. Three independent experiments were performed and repeated at least three times.

## Transmission Electron Microscopy (TEM)

DU145 and PC3 cells were sequentially fixed with 2.5% glutaraldehyde and 1% sodium dihydrogen phosphate and then postfixed with 1% osmium tetroxide. Ultrathin sections were obtained using a microtome, and autophagosomes and CNPs were then observed.

## Multifactor Detection of a Single Akt Phosphorylation Pathway

Cell extraction was measured by RayBio Human/Mouse *AKT* Pathway Phosphorylation Array C1 (Raybiotech, Inc., Georgia, USA) which simultaneously detected 18 phosphorylated human or mouse proteins using multiplexed sandwich ELISA-based technology. The experiment was performed by Raybiotech, Inc. (Guangzhou, China) according to the manufacturer's instructions. Briefly, the membranes were blocked with blocking buffer for 30 min at room temperature. Then, 1mL 500 μg/mL cell extraction was pipetted into each membrane and incubated with primary antibodies at 4 °C overnight. The membranes were then washed with wash buffer twice and incubated with 1× HRP-anti-rabbit IgG for 2 h at room temperature. Subsequently, a detection buffer mixture was added to the membranes, which were illustrated using a chemiluminescence imaging system.

## Immunohistochemistry (IHC)

Tissue samples were deparaffinized with xylene, and an UltraSensitiveTM SP (Mouse/Rabbit) IHC kit (KIT-9730, MX Biotechnologies) was used for detection. After proteolytic digestion and peroxidase blocking, the tissue specimens were incubated with anti-*Caspase-3* (#9664S, Cell Signaling Technology), anti-*Cleaved Caspase-3* (#9662, Cell Signaling Technology), anti-*SQSTM1* (sc-48402, Santa Cruz), anti-*4E-BP1* (#9452, Cell Signaling Technology), anti-*Vimentin* (A19607, ABclonal), and anti-*E-Cadherin* (#3195T, Cell Signaling Technology) antibodies at a dilution of 1:200. The biotinylated secondary antibodies in the kit were used according to the manufacturer's instructions after washing the samples. Then, the samples were washed with PBS three times and then incubated with streptavidin-horseradish peroxidase complex. A DAB substrate kit was used for staining. Liver tissues from control group mice were used as positive and negative control. Negative controls were prepared by substituting with normal rabbit or mouse IgG.[19] The immunoreactivity scores were calculated by two pathologists using a system based on multiplying the staining percentage (0: 0–5%, 1: 6–25%, 2: 26–50%, 3: 51–75% and 4: 76–100%) and intensity (0: negative, 1: weak, 2: moderate and 3: strong).

## Animal Experiments

The Institute for Laboratory Animal Research at Guangzhou Medical University, Guangzhou, PR China, approved all animal protocols. Animal experiments were performed with the guidelines of the Institute for Laboratory Animal Research at Guangzhou Medical University, Guangzhou, China. Sixteen male *BALB/c nude mice* were subcutaneously injected with $5 \times 10^7$ DU145 or PC3 cells on the right side of the back. Tumor volume [volume $(mm^3) = 0.5 \times$ length $(mm) \times$ width$^2$ $(mm^2)$] was calculated every three days. A local subcutaneous injection of 5 mg of CNPs was performed every three days among eight of the sixteen mice. Fourteen days after the injection, tumor tissue samples were used for Western blotting and IHC.

## Statistical Analysis

The data are presented as the means ± standard deviation (SD). Statistical analysis was conducted by an independent-sample $t$-test using SPSS v16 and GraphPad Prism 8.

The results were considered as statistically significant if \*P < 0.05 or \*\*P < 0.01.

# Results

## Morphologies and Structure of CNPs

In addition to CNPs, carbon nanotubes (CNTs) were used in the current study as a control group. We confirmed the morphologies and structure of the CNPs by SEM at different magnifications. Figure 1A shows that these nanomaterials were uniformly sized, spherical materials. The diameter of the CNPs was 450 nm, while the diameter of the carbon nanotubes was approximately 100–1,000 nm (Figure 1B). The CNPs had XRD results similar to those of the carbon nanotubes (Figure 1D), which confirmed that both of these materials exhibited a phase composition of carbon, but a smaller zeta potential value (Figure 1C). These results were predicted to indicate similar but somewhat poor physical stability of CNPs. To improve solubility, CNPs diluted with DMSO were used in this study. A Raman scattering spectrum showed Raman peaks at 1,300 and 1,580 $cm^{-1}$, corresponding to the vibrational modes of $D^-$ and $G^-$ (Figure 1E). Overall, CNPs have some similarities to CNTs, but the two materials have different shapes. The carbon nanomaterials used in this study, both the CNPs and CNTs, were pure, with sizes of 450 nm and approximately 100–1,000 nm, respectively.

## Antitumor Effect of CNPs on PCa Cells in vitro
### CNPs Inhibit Cell Growth and the Cell Cycle in PCa Cells

The two PCa cell lines DU145 and PC3 were used in this study, both of which were treated with 5 and 10 μg/mL of CNPs. The CCK-8 assay results showed that CNPs inhibited the growth of the PC3 and DU145 cell lines, while no effect on the benign prostate epithelial cells BPH-1 was observed (Figure 2A). The impacts of CNPs on these PCa cells were density-dependent. Therefore, we believe that CNPs specifically affected PCa but not normal cells. Considering the enhanced effect without apparent deposition observed, CNPs were used at a dose of 10 μg/mL in the following experiments.

To further assess the effect of CNPs on cell proliferation, we investigated the cell cycle by flow cytometric analysis (Figure 2B). Compared to control cells, DU145 and PC3 cells treated with CNPs were arrested in the G1 phase, showing that DNA duplication and synthesis were reduced. The percentage of cells in the G1 phases increased from 59.947±0.577% to 64.84±0.129% in DU145 cells and from 54.743±0.282% to 60.673 ±1.074% in PC3 cells after treatment with CNPs.

## CNPs Inhibit PCa Cell Migration and Invasion

Relatively aggressive growth, progression, and metastasis are features of cancers. After observing the CNP-mediated suppression of PCa cells, we then investigated the effects of CNPs on the invasive and migratory abilities of two types of PCa cells through Transwell and wound-healing experiments. The results shown in Figure 3 indicate that CNPs significantly inhibited cell invasion (Figure 3A and B) and migration (Figure 3C and D) in the CNP-treated group compared with the control group. The migration distances of the DU145 and PC3 cells treated with the CNPs were 1.000±0.000 vs 0.737±0.003 and 1.000±0.000 vs 0.791±0.022, respectively.

## CNPs Induce Apoptosis and Autophagy in PCa Cells

Changes in cell number can be occurred due to cell proliferation or death. The experiments above showed that the number of PCa cells and level of DNA synthesis decreased following the addition of CNPs. To further explore the impact of this nanomaterial on cell death, we evaluated changes in apoptosis and autophagy in vitro. According to our Western blot results, the expression of *Cleaved Caspase-3*, which is derived from *Caspase-3* and used as an apoptosis marker,[20] increased after treatment with CNPs (Figure 4A). Furthermore, flow cytometry results (Figure 4B) also showed that CNP treatment increased the proportions of cells in both the early and late stages of apoptosis. These results confirmed that the CNPs induced apoptosis in PCa cells.

SQSTM1 has been reported to have a negative correlation with the proteasome and autophagic flux, and this protein can be used to detect autophagy with *LC 3* (another autophagy marker).[21–23] The ratio of *LC3 II* to *LC3 I* increased, while the expression of *SQSTM1* decreased in the CNPs group compared with the control group (Figure 4A). Because *LC3 II* can be degraded in the autolysosomal lumen, which can cause inaccurate measurements of the autophagy rate, bafilomycin a1 (Baf-A1; 88899–55-2, Sigma-Aldrich, USA) was used to interrupt autophagic flux and aid in detecting autophagy.[24] The same trend in the level of *LC3 II* was observed in the CNPs group in the presence of Baf-A1 (Figure 4A). CNPs and more autophagosomes, which could also be identified
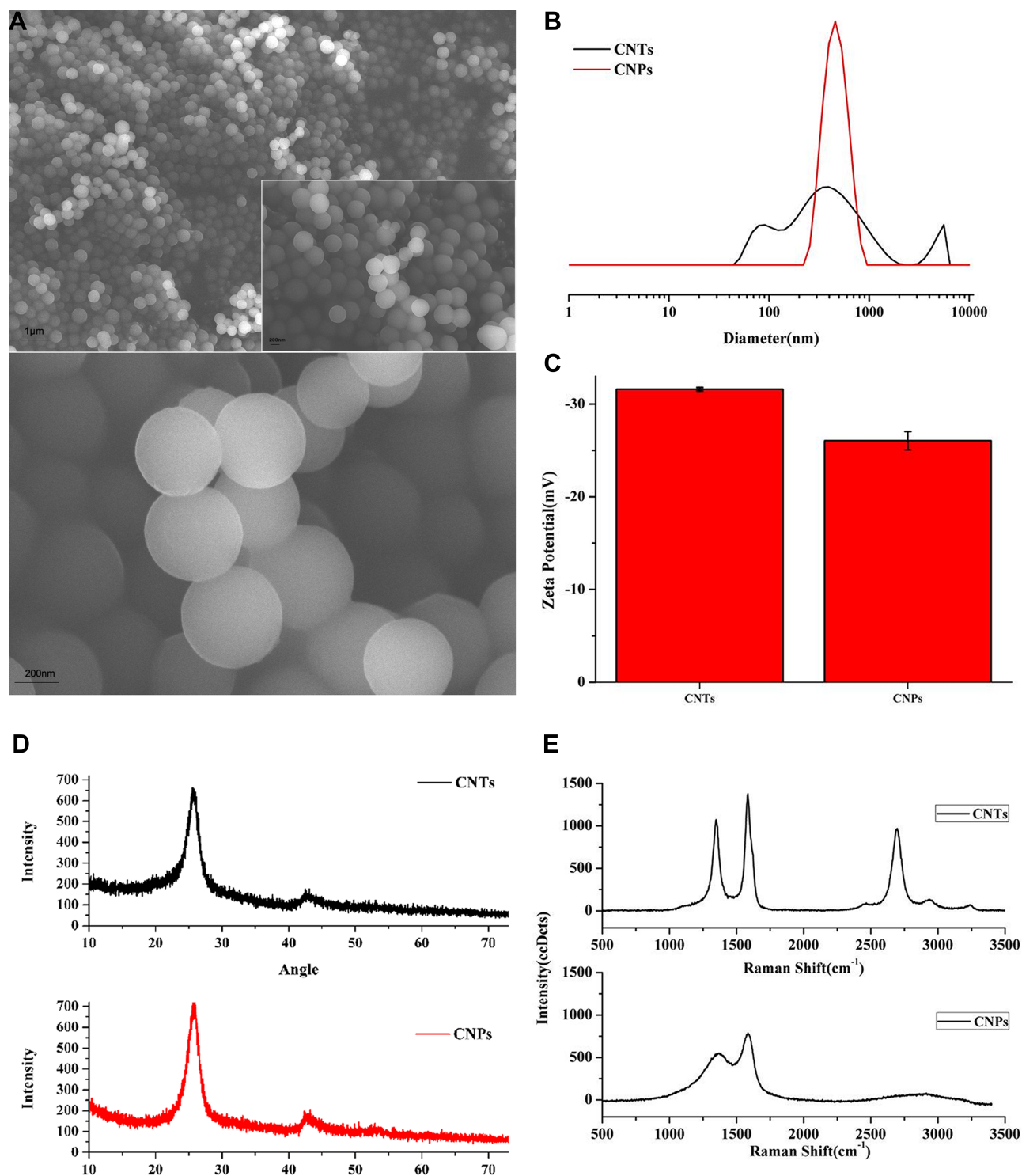
**Figure 1** Characterization of carbon nanospheres and carbon nanotubes. (**A**) SEM images of carbon nanospheres. (**B**) Diameters of carbon nanospheres and carbon nanotubes. (**C**) Zeta potentials of carbon nanospheres and carbon nanotubes. (**D**) XRD patterns of carbon nanospheres and carbon nanotubes. (**E**) Raman spectra of carbon nanotubes and carbon spheres.

by TEM, were observed in cells treated with CNPs compared to that observed in the control cells (Figure 4C).

The *PI3K/AKT/mTOR* pathway is one of the most well studied and crucial signaling pathways involved in regulating cell death. To further elucidate the mechanism underlying CNP-induced apoptosis and autophagy, multifactor detection of a single *Akt* phosphorylation pathway was used in the present study. The results showed that
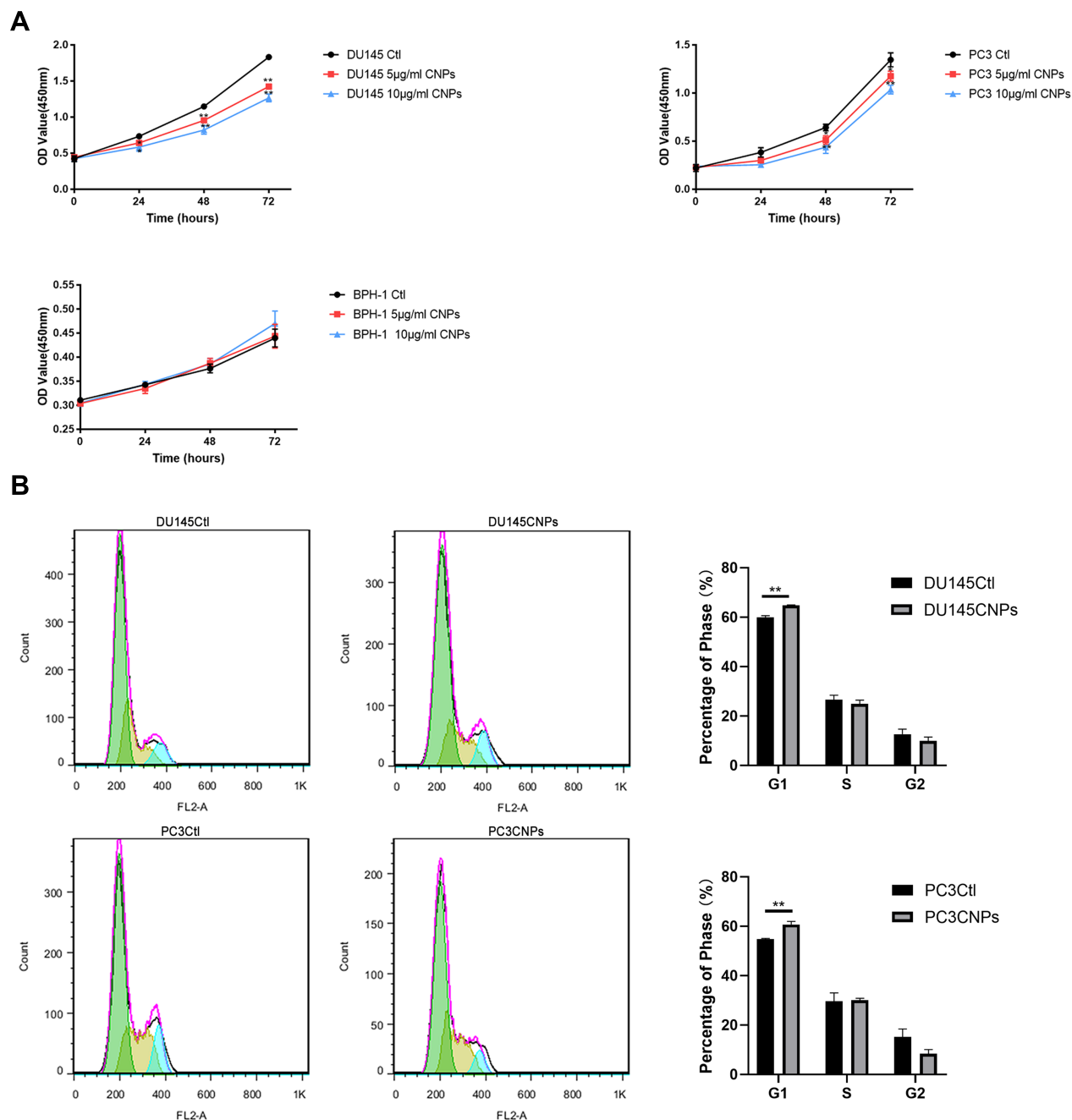
**Figure 2** CNPs inhibit the cell growth of PCa cell lines in vitro. (**A**) A CCK-8 assay. (**B**) Cell cycle analysis. The data are presented as the means ± SD of three independent experiments. *P<0.05, **P<0.01.

there were six differentially expressed proteins in DU145 cells, including *PRAS40*, *4E-BP1*, *RSK1*, *mTOR*, *BAD*, and *AMPKa* and five differentially expressed proteins in PC3 cells, including *4E-BP1*, *RPS6*, *Erk1/2*, *PDK1*, and *Raf-1* when comparing the CNPs group with the control group (Figure 5A). Kyoto Encyclopedia of Genes and Genomes (KEGG) pathway analysis revealed that CNPs may be associated with the mTOR pathway and insulin pathway in PCa (Figure 5B). In addition, *4E-BP1* was

downregulated in both cell lines. Then, we verified that the CNPs inhibited the expression of *4E-BP1* by Western blot analysis in DU145 and PC3 cells (Figure 5C).

## Antitumor Effect of CNPs on PCa Cells in vivo

To investigate the impact of the CNPs in vivo, DU145 and PC3 cells were locally and subcutaneously inoculated into
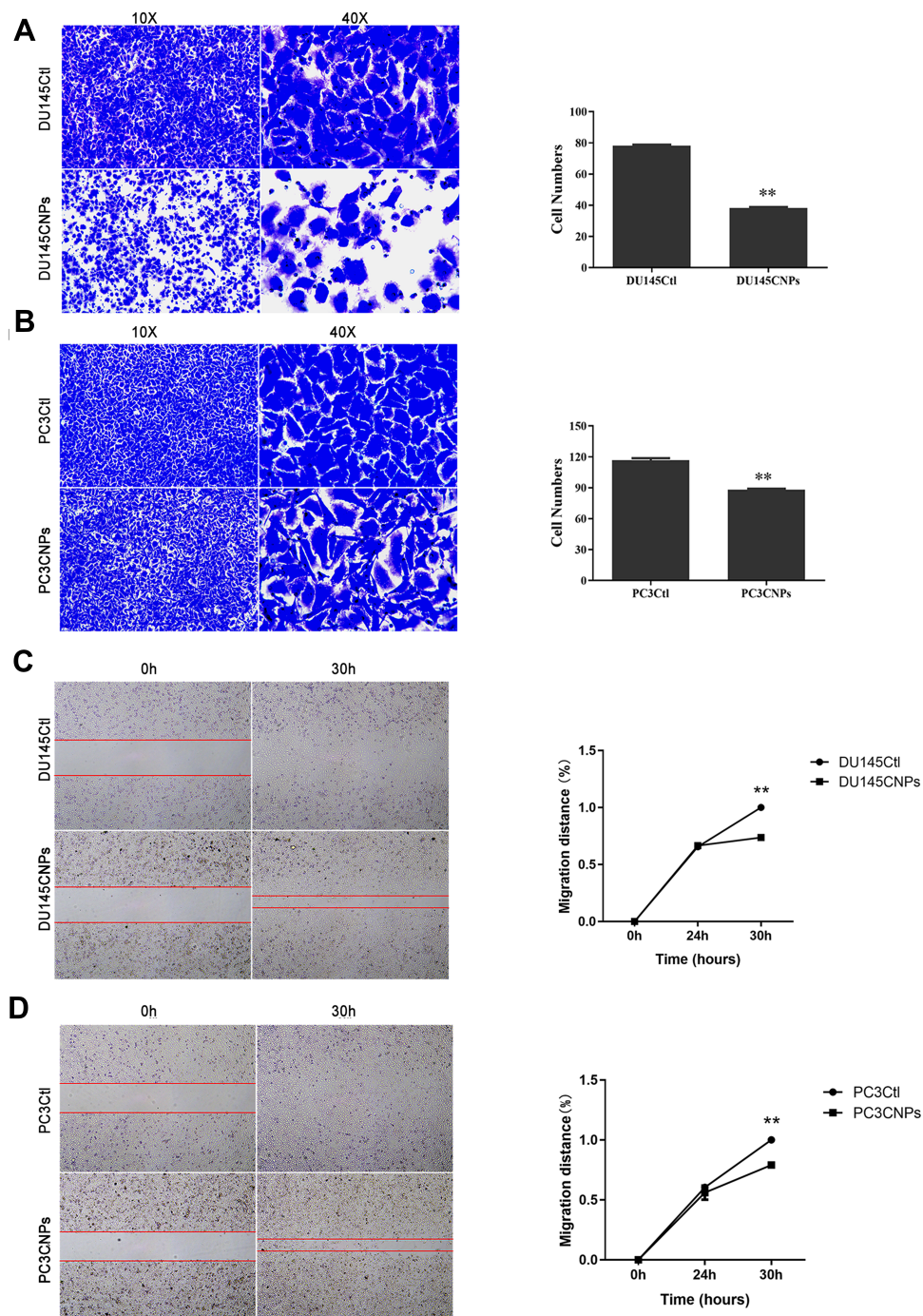
**Figure 3** Carbon nanospheres inhibit the invasion and migration of PCa cell lines. Invasion of (**A**) DU145 and (**B**) PC3 cells determined by Transwell assays. Migration of (**C**) DU145 and (**D**) PC3 cells determined by a wound-healing assay. The data are presented as the means ± SD of three independent experiments. **p<0.01.

nude mice. The percentage change of volume per day in a tumor, also known as the tumor growth rate, was used to describe the CNPs' effect on PCa.[25] The tumor growth rate was significantly reduced when the CNPs were injected (Figure 6B). Tumor volumes were smaller for the CNP-treated tumors than the control tumors, and the CNPs accumulated in the tumor tissue (Figure 6A). Therefore,

we assume that the carbon nanospheres inhibited prostate cell growth in vivo.

After the injection of CNPs, the expression of *E-Cadherin* (Figure 7A and C) and *Vimentin* (Figure 7B and C) was evaluated by IHC and Western blotting. *E-Cadherin* was expressed in PC3 but not in DU145 cells, while *Vimentin* was expressed in DU145 but not
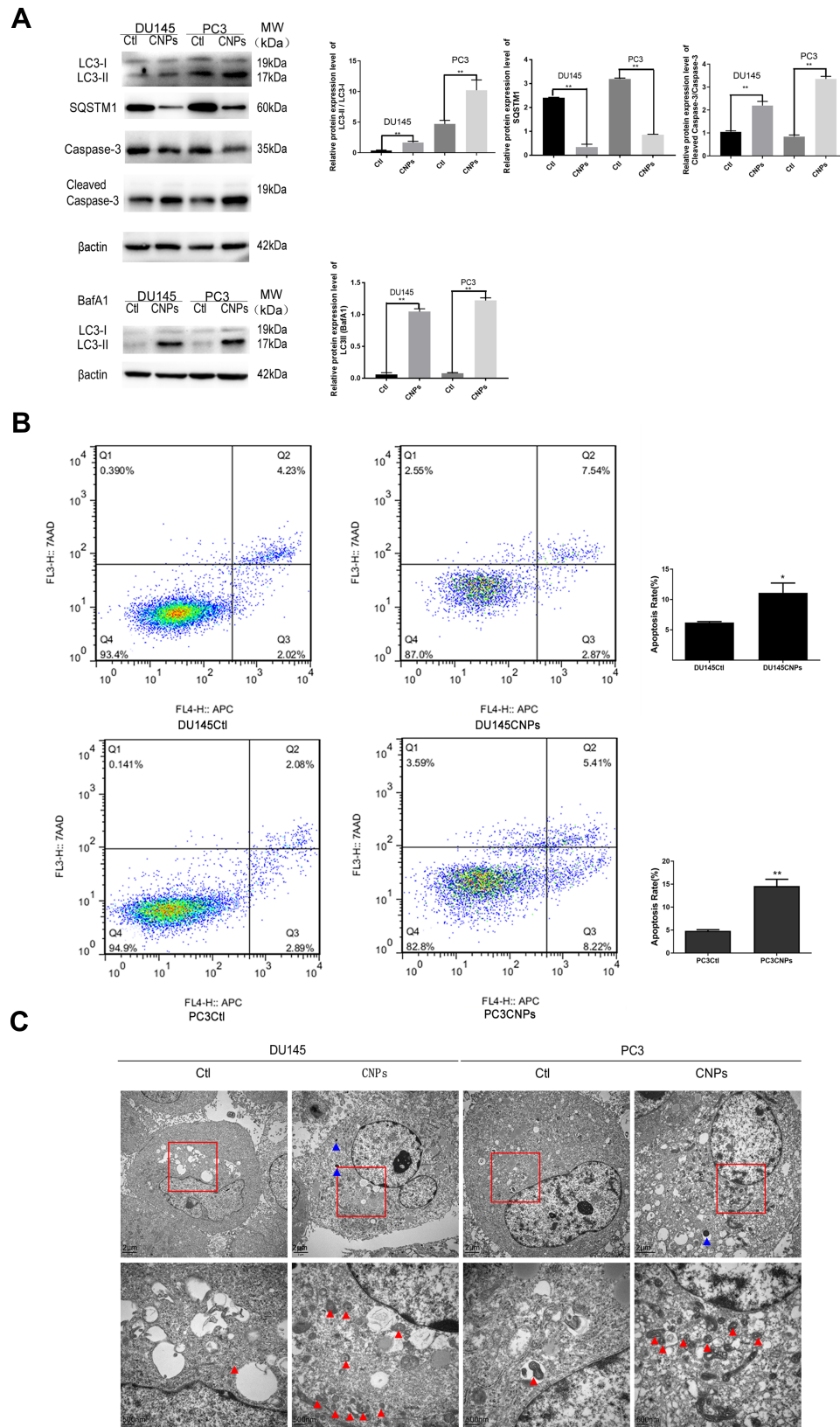
**Figure 4** Carbon nanospheres promote autophagy and induce apoptosis of PCa cell lines in-vitro. (**A**) Protein expression levels of *Cleaved Caspase-3* and *Caspase-3*, *SQSTM1*, and *LC3 I/II* in cells treated or not treated with Baf-A1 after incubating with CNPs. (**B**) Cell apoptosis assay results. (**C**) Transmission electron microscopy images of CNPs (blue triangle) and autophagosomes (red triangle) in PCa cells. The data are presented as the means ± SD of three independent experiments. *P<0.05, **P<0.01.

A

**DU145**

| proteinID | AveExp.CNPs | AveExp.Ctl | logFC | foldchange | regulation |
|---|---|---|---|---|---|
| PRAS40 | 14.01 | 14.50 | −0.49 | 0.71 | down |
| 4E−BP1 | 15.02 | 15.38 | −0.36 | 0.78 | down |
| RSK1 | 13.77 | 14.09 | −0.32 | 0.80 | down |
| mTor | 13.65 | 13.95 | −0.30 | 0.81 | down |
| BAD | 14.03 | 14.32 | −0.29 | 0.82 | down |
| AMPKa | 14.52 | 14.79 | −0.27 | 0.83 | down |

**PC3**

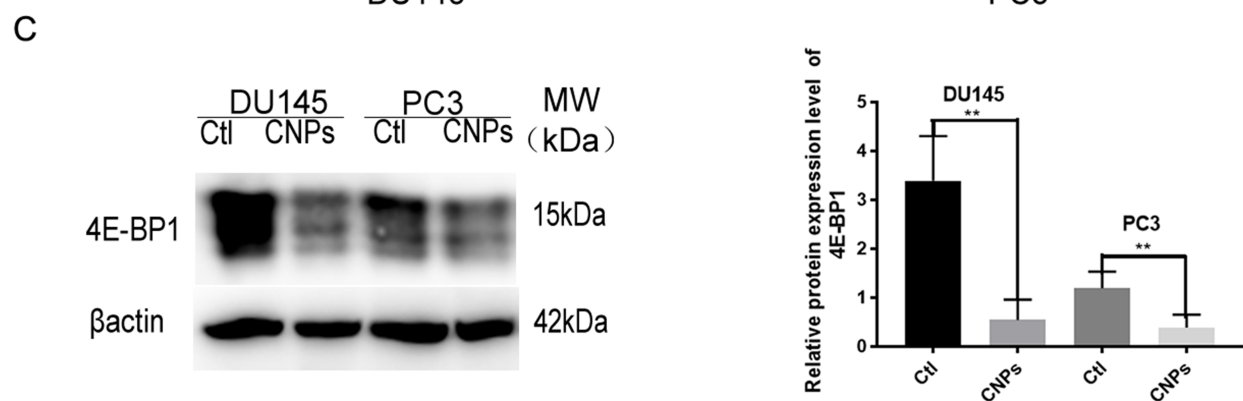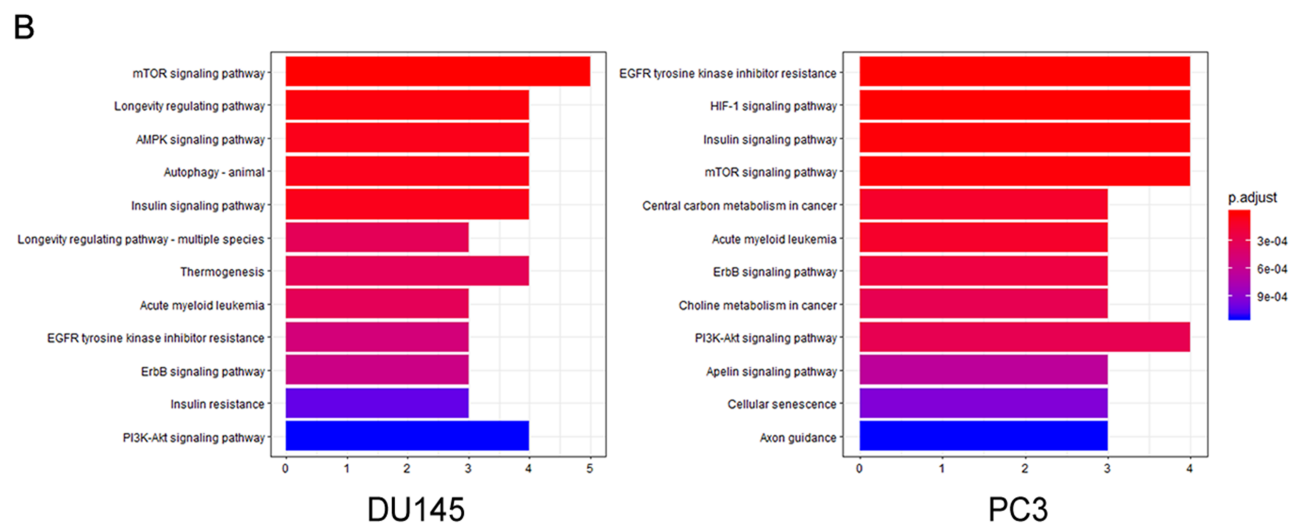| proteinID | AveExp.CNPs | AveExp.Ctl | logFC | foldchange | regulation |
|---|---|---|---|---|---|
| 4E-BP1 | 13.74 | 14.06 | −0.32 | 0.80 | down |
| RPS6 | 12.89 | 12.59 | 0.30 | 1.23 | up |
| Erk1/2 | 12.17 | 11.83 | 0.34 | 1.26 | up |
| PDK1 | 13.29 | 12.86 | 0.43 | 1.34 | up |
| Raf-1 | 12.69 | 12.26 | 0.43 | 1.35 | up |

B



C



**Figure 5** Validation of differentially expressed proteins. (**A**) Conservative analysis of different proteins. (**B**) KEGG pathways of the identified differentially expressed proteins. (**C**) Quantification of the relative intensities of *4E-BP1* represented as a histogram. **P<0.01.
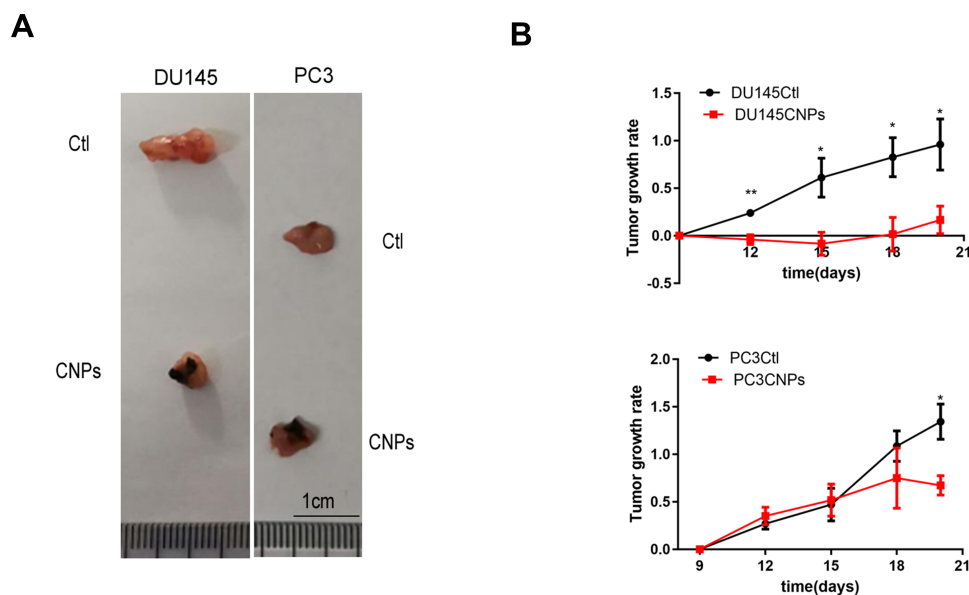
**A**



**B**



**Figure 6** Carbon nanospheres inhibit PCa tumor growth in vivo. (**A**) Tumors from the animal models are shown. (**B**) Tumor growth rates were determined. *P<0.05, **P<0.01.

PC3 cells. The IHC score for *E-Cadherin* in PC3 cells was higher in the CNPs group than that observed in the control group, and the expression of *E-Cadherin* was also higher in the CNPs group according to the Western blot results. In contrast, the IHC score for *Vimentin* in DU145 cells was lower in the CNPs group than that observed in the control group, and its expression was also lower in the same group according to the Western blot results. The observed upregulation of *E-Cadherin* expression and downregulation of *Vimentin* expression suggests that the CNPs inhibited epithelial-mesenchymal transition (EMT), which may lead to the suppression of invasion and metastasis in PCa.[26]

The expression of *Caspase-3* and *Cleaved Caspase-3* were tested in prostate tumor tissue (Figure 8 and Supplementary Figure S1). The IHC scores and the protein expression of *Cleaved Caspase-3* (Figure 8A) were higher in the CNPs group than those observed in the control group, while there was no significant difference in the expression of *Caspase-3* (Supplementary Figure S1) between these two groups, indicating that the CNPs induce apoptosis in PCa. The same trend was also observed by the Western blot results (Figure 8B).

To detect changes in autophagy in prostate tumor tissues, *4E-BP1* and *SQSTM1* levels were measured by both IHC and Western blotting. The CNPs group had higher IHC scores for *4E-BP1* and *SQSTM1* than was observed in the control group (Figure 9A and B). We obtained the same result by evaluating the protein level by Western blotting (Figure 9C), with lower expression of *4E-BP1*, *SQSTM1* and higher expression of *LC3 II/I* observed in the CNPs group than that detected in the control group. We observed an accumulation of CNPs and increased numbers of autophagosomes with the injection of the material into prostate cancer tissues (Figure 9D). Positive control IHC results of *Caspase-3*, *Cleaved Caspase-3*, and both positive and negative control of *SQSTM1* were presented in Supplementary Figure S2. Overall, consistent with our in vitro work, we observed that the CNPs induced apoptosis and autophagy, which may lead to downregulation of *4E-BP1* expression in vivo.

## Discussion

It is much easier for nanomaterials to accumulate in tumors with abundant blood flow, gaps in blood vessel walls and poor lymphatic circulation than in other tissues in vivo. This phenomenon is called the enhanced permeability and retention effect.[27,28] Nanomaterials are widely used in the diagnosis and treatment of diseases, especially in the field of autophagy-related cancer treatment.[29–32] By using materials with individual functions related to sound, light, electricity, heat, etc., nanomaterials can be used to deliver a drug to a particular part of the body with an excellent drug loading efficiency while simultaneously reducing the possibility of drug resistance.[33,34]
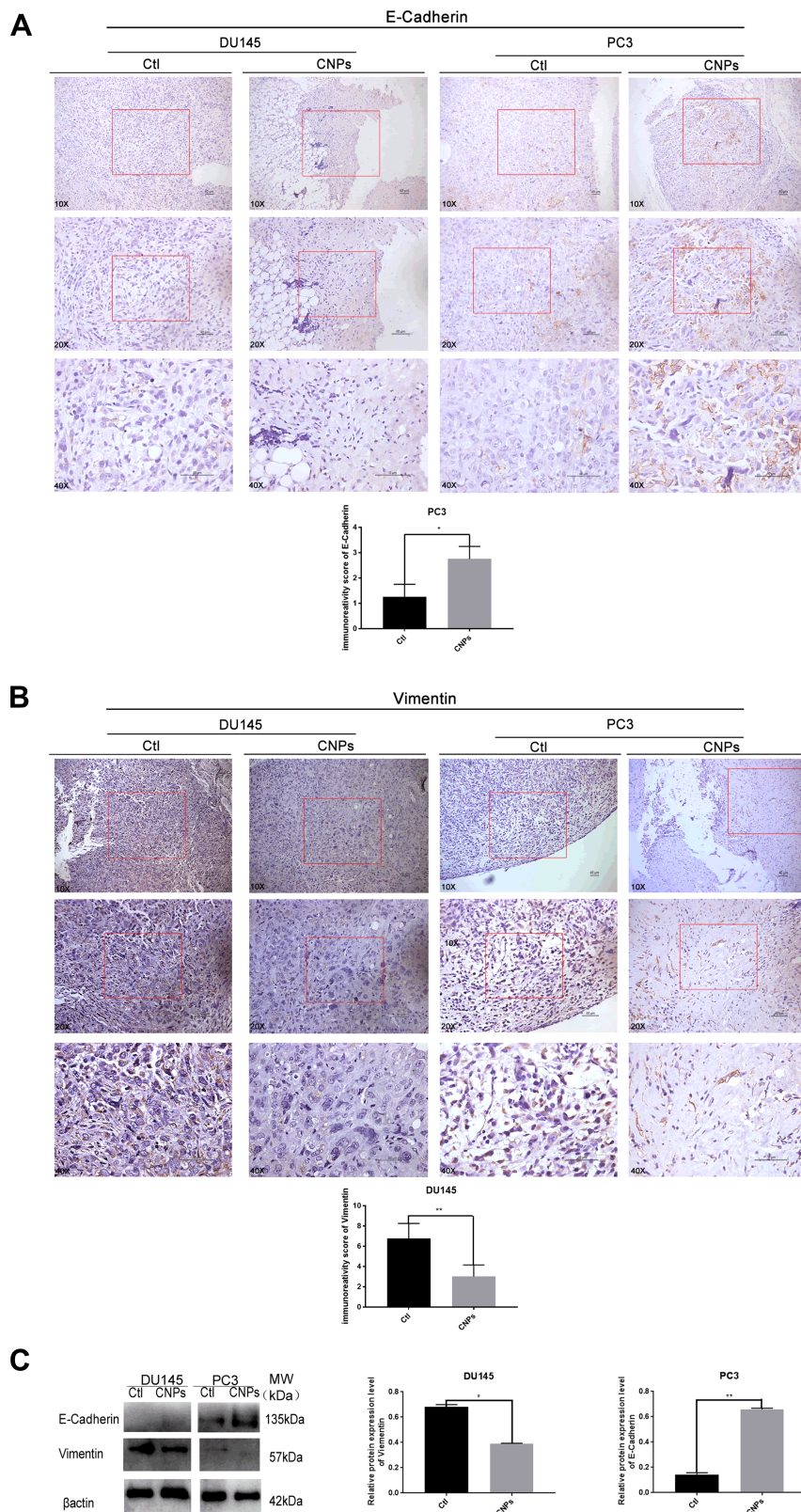
**Figure 7** Carbon nanospheres inhibit EMT in vivo. Protein expression levels of (**A**) *E-Cadherin* and (**B**) *Vimentin* in the tumor xenografts established with DU145 and PC3 cells in the CNP and negative control groups. (**C**) *E-Cadherin* and *Vimentin* were also assessed by Western blotting. *P<0.05 and **P9<0.01.
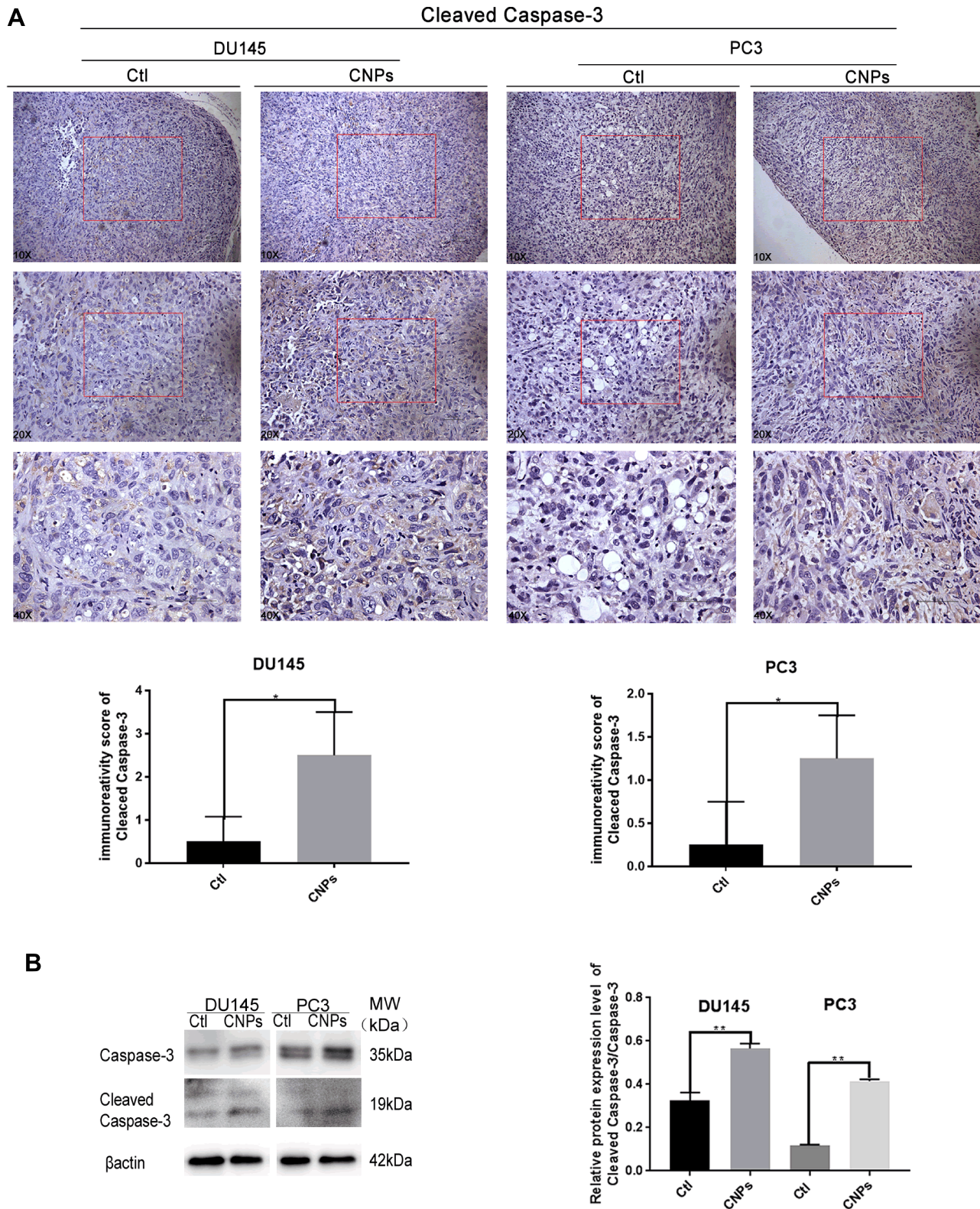
**Figure 8** Carbon nanospheres promote apoptosis in vivo. (**A**) *Cleaved Caspase-3* expression was increased. Representative immunohistochemical staining for *Cleaved Caspase-3* is shown. (**B**) The ratio of *Cleaved Caspase-3* to *Caspase-3* was assessed by Western blotting. *P<0.05 and **P<0.01.
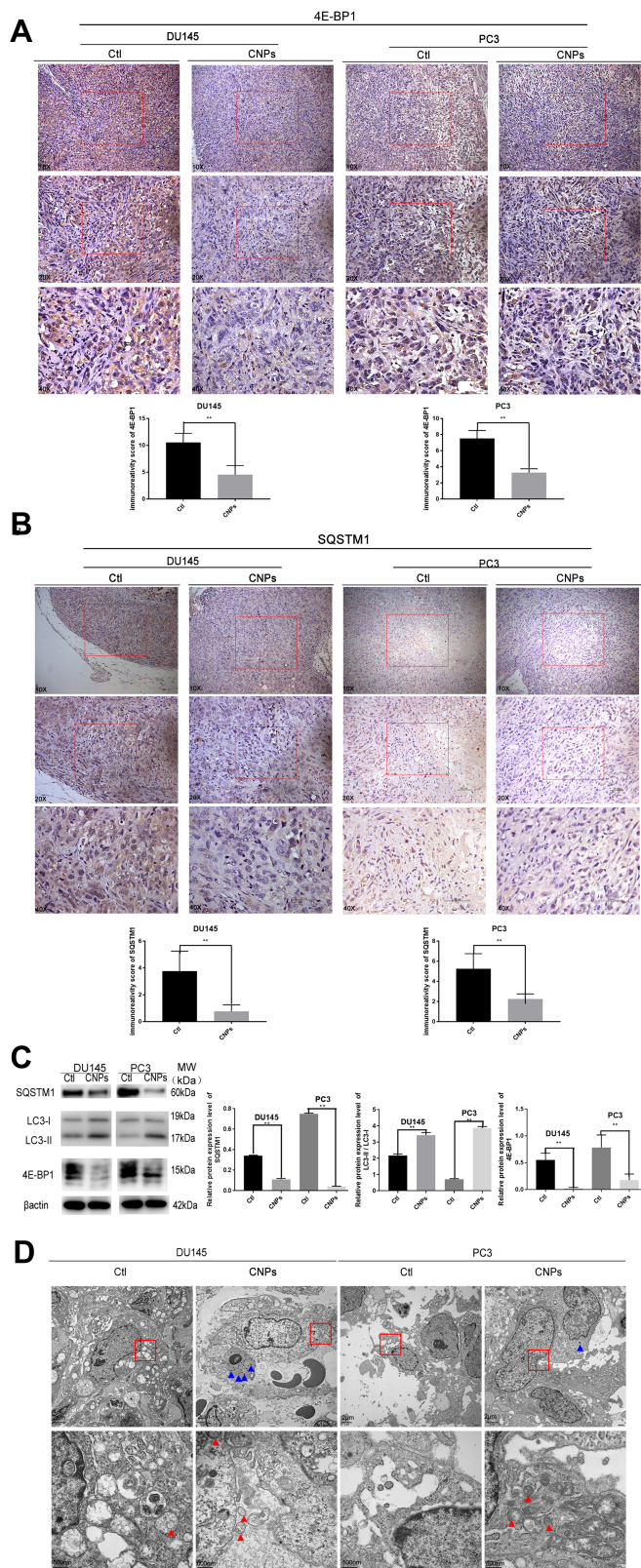
**Figure 9** Carbon nanospheres promote autophagy in vivo. Protein expression levels of (**A**) *4E-BP1* and (**B**) *SQSTM1* in the tumor xenografts established with PCa cells in CNPs and negative control groups. (**C**) *4E-BP1*, *SQSTM1*, and *LC3 I/II* levels were assessed by Western Blot. (**D**) Transmission electron microscopy images of prostate cancer in vitro. **P<0.01.

Among all carbon nanomaterials, CNTs have been used to deliver small interfering RNAs (siRNAs) and polyethyleneimine-functionalized CNTs have been used to deliver siRNAs into human cervical cancer cells.[35] Recently, nanocarbon tubes were successfully used to target CpGODN in the PCa immunotherapy.[36] Although research on carbon nanomaterials for drug or gene delivery is not uncommon, few studies have explored their effects in vivo. In addition, the material used for synthesis of CNP, glucose, is inexpensive and abundant.[15] The synthetic method is easy and environmentally friendly, and considering these advantages, the future of CNPs is bright.

Our results demonstrated that the anticancer effects of CNPs, including inhibition of growth, proliferation, metastasis, and invasion in PCa cells in vivo and in vitro. We also observed that CNPs induced apoptosis and autophagy and downregulated *4E-BP1* expression in PCa. Nanomaterial loading of an mTOR inhibitor inhibited the expression of *4E-BP1* in B lymphoma cells.[37] However, there is no satisfactory research on nanomaterials without contents assessing changes in *4E-BP1* levels. *4E-BP1* is a downstream effector of *mTOR*,[38] and its expression is higher in PCa tissue than in normal tissue.[39] *4E-BP1* inhibition may induce apoptosis and autophagy.[40,41] These findings are consistent with our conclusions, and the downregulation of *4E-BP1* expression likely indicates a possible signaling pathway involved in the CNP induced antitumor effect. In addition, we observed that CNPs inhibited PCa cell growth but not benign prostate epithelial cell growth. These results suggest that CNPs could be a carbon nanomaterial for selective killing of PCa cells, which needs to be confirmed in further research. Currently, the interaction of the nanomaterial itself with tumors remains unelucidated. Few nanomaterials are used in the clinic due to a lack of knowledge regarding the mechanisms of nanomaterials in the human body. In addition to promising drug and delivery functions, CNPs can also act as a potential treatment in PCa.

## Funding

## Disclosure

The authors declare no conflicts of interest for this work.

## References

1. Siegel RL, Miller KD, Jemal A. Cancer statistics, 2019. *CA Cancer J Clin*. 2019;69(1):7–34. doi:10.3322/caac.21551
2. Mottet N, Bellmunt J, Bolla M, et al. EAU-ESTRO-SIOG guidelines on prostate cancer. Part 1: screening, diagnosis, and local treatment with curative intent. *Eur Urol*. 2017;71(4):618–629. doi:10.1016/j.eururo.2016.08.003
3. Raina R, Lakin MM, Agarwal A, et al. Long-term effect of sildenafil citrate on erectile dysfunction after radical prostatectomy: 3-year follow-up. *Urology*. 2003;62(1):110–115. doi:10.1016/S0090-4295(03)00157-2
4. Bar-Zeev M, Livney YD, Assaraf YG. Targeted nanomedicine for cancer therapeutics: towards precision medicine overcoming drug resistance. *Drug Resist Updat*. 2017;31:15–30. doi:10.1016/j.drup.2017.05.002
5. Zhang M, Wang W, Wu F, Graveran K, Zhang J, Wu C. Black phosphorus quantum dots gated, carbon-coated Fe3O4 nanocapsules (BPQDs@ ss-Fe3O4@ C) with low premature release could enable imaging-guided cancer combination therapy. *Chem a Eur J*. 2018;24(49):12890–12901. doi:10.1002/chem.201801085
6. Zhang M, Sheng B, Ashley J, et al. Manganese ion chelated FeOCl@ PB@ PDA@ BPQDs nanocomposites as a tumor microenvironment-mediated nanoplatform for enhanced tumor imaging and therapy. *Sens Actuators B Chem*. 2020;307:127491. doi:10.1016/j.snb.2019.127491
7. Islam MA, Xu Y, Tao W, et al. Author correction: restoration of tumour-growth suppression in vivo via systemic nanoparticle-mediated delivery of PTEN mRNA. *Nat Biomed Eng*. 2018;2(12):968. doi:10.1038/s41551-018-0331-x
8. Kesharwani P, Iyer AK. Recent advances in dendrimer-based nanovectors for tumor-targeted drug and gene delivery. *Drug Discov Today*. 2015;20(5):536–547. doi:10.1016/j.drudis.2014.12.012
9. Li X, Wu M, Pan L, Shi J. Tumor vascular-targeted co-delivery of anti-angiogenesis and chemotherapeutic agents by mesoporous silica nanoparticle-based drug delivery system for synergetic therapy of tumor. *Int J Nanomedicine*. 2016;11:93.
10. Kroto H. The birth of C 60: buckminsterfullerene. In: *Electronic Properties of Fullerenes*. Springer; 1993:1–7.
11. Ji S-R, Liu C, Zhang B, et al. Carbon nanotubes in cancer diagnosis and therapy. *Biochim Biophys Acta*. 2010;1806(1):29–35. doi:10.1016/j.bbcan.2010.02.004
12. Pan M, Annamalai K, Tao Y. Applications of nanocarbons in bio-medical devices. *Recent Innov Chem Eng*. 2015;8(2):67–74.
13. Juzgado A, Soldà A, Ostric A, et al. Highly sensitive electrochemiluminescence detection of a prostate cancer biomarker. *J Mater Chem B*. 2017;5(32):6681–6687. doi:10.1039/C7TB01557G
14. Nieto-Márquez A, Romero R, Romero A, Valverde JL. Carbon nanospheres: synthesis, physicochemical properties and applications. *J Mater Chem*. 2011;21(6):1664–1672. doi:10.1039/C0JM01350A
15. Zhang P, Qiao Z-A Z-A, Dai S. Recent advances in carbon nanospheres: synthetic routes and applications. *Chem Comm*. 2015;51(45):9246–9256. doi:10.1039/C5CC01759A
16. DeSantis M, Bowne W, Ferretti J, Franceschi A. Long term evaluation of mouse toxicity using application of spherical nanocarbon injected into known human prostatic carcinoma in nude mouse with microwave assisted therapy. *J Nucl Med*. 2014;55(supplement 1):1515.
17. Mi Y, Hu W, Dan Y, Liu Y. Synthesis of carbon micro-spheres by a glucose hydrothermal method. *Mater Lett*. 2008;62(8–9):1194–1196. doi:10.1016/j.matlet.2007.08.011
18. Jia Zhuo Y, Zhen Liu Z, Wan S, et al. Enhanced expression of SRPK2 contributes to aggressive progression and metastasis in prostate cancer. *Biomed Pharmacother*. 2018;102:531–538. doi:10.1016/j.biopha.2018.03.079

19. Hewitt SM, Baskin DG, Frevert CW, Stahl WL, Rosa-Molinar E. Controls for immunohistochemistry: the histochemical society's standards of practice for validation of immunohistochemical assays. *J Histochem Cytochem*. 2014;62(10):693–697. doi:10.1369/0022155414545224

20. Martinez MM, Reif RD, Pappas D. Detection of apoptosis: a review of conventional and novel techniques. *Anal Methods*. 2010;2(8):996–1004. doi:10.1039/c0ay00247j

21. Deretic V. Autophagosome and phagosome. In: *Autophagosome and Phagosome*. Springer; 2008:1–10.

22. Bjørkøy G, Lamark T, Pankiv S, Øvervatn A, Brech A, Johansen T. Monitoring autophagic degradation of p62/SQSTM1. *Methods Enzymol*. 2009;452:181–197.

23. Puissant A, Fenouille N, Auberger P. When autophagy meets cancer through p62/SQSTM1. *Am J Cancer Res*. 2012;2(4):397.

24. Klionsky DJ, Elazar Z, Seglen PO, Rubinsztein DC. *Does Bafilomycin A1 Block the Fusion of Autophagosomes with Lysosomes?* Taylor & Francis; 2008.

25. Mehrara E, Forssell-Aronsson E, Ahlman H, Bernhardt P. Specific growth rate versus doubling time for quantitative characterization of tumor growth rate. *Cancer Res*. 2007;67(8):3970–3975. doi:10.1158/0008-5472.CAN-06-3822

26. Sethi S, Macoska J, Chen W, Sarkar FH. Molecular signature of epithelial-mesenchymal transition (EMT) in human prostate cancer bone metastasis. *Am J Transl Res*. 2011;3(1):90.

27. Iyer AK, Khaled G, Fang J, Maeda H. Exploiting the enhanced permeability and retention effect for tumor targeting. *Drug Discov Today*. 2006;11(17–18):812–818. doi:10.1016/j.drudis.2006.07.005

28. Maeda H, Tsukigawa K, Fang J. A retrospective 30 years after discovery of the enhanced permeability and retention effect of solid tumors: next-generation chemotherapeutics and photodynamic therapy—problems, solutions, and prospects. *Microcirculation*. 2016;23(3):173–182. doi:10.1111/micc.12228

29. Zhang Q, Yang W, Man N, et al. Autophagy-mediated chemosensitization in cancer cells by fullerene C60 nanocrystal. *Autophagy*. 2009;5(8):1107–1117. doi:10.4161/auto.5.8.9842

30. Panzarini E, Inguscio V, Tenuzzo BA, Carata E, Dini L. Nanomaterials and autophagy: new insights in cancer treatment. *Cancers*. 2013;5(1):296–319. doi:10.3390/cancers5010296

31. Panzarini E, Dini L. Nanomaterial-induced autophagy: a new reversal MDR tool in cancer therapy? *Mol Pharm*. 2014;11(8):2527–2538. doi:10.1021/mp500066v

32. Li J, Yang S, Deng Y, et al. Emancipating target-functionalized carbon dots from autophagy vesicles for a novel visualized tumor therapy. *Adv Funct Mater*. 2018;28(30):1800881. doi:10.1002/adfm.201800881

33. Schodek DL, Ferreira P, Ashby MF. *Nanomaterials, Nanotechnologies and Design: An Introduction for Engineers and Architects*. Butterworth-Heinemann; 2009.

34. Shin T-H, Cheon J. Synergism of nanomaterials with physical stimuli for biology and medicine. *Acc Chem Res*. 2017;50(3):567–572. doi:10.1021/acs.accounts.6b00559

35. Huang Y-P, Lin I-J, Chen -C-C, Hsu Y-C, Chang -C-C, Lee M-J. Delivery of small interfering RNAs in human cervical cancer cells by polyethylenimine-functionalized carbon nanotubes. *Nanoscale Res Lett*. 2013;8(1):1–11. doi:10.1186/1556-276X-8-267

36. Xia Q, Gong C, Gu F, et al. Functionalized multi-walled carbon nanotubes for targeting delivery of immunostimulatory CpG oligonucleotides against prostate cancer. *J Biomed Nanotechnol*. 2018;14(9):1613–1626. doi:10.1166/jbn.2018.2605

37. Tang X, Xie C, Jiang Z, et al. Rituximab (anti-CD20)-modified AZD-2014-encapsulated nanoparticles killing of B lymphoma cells. *Artif Cells Nanomed Biotechno*. 2018;46(sup2):1063–1073. doi:10.1080/21691401.2018.1478844

38. Fingar DC, Richardson CJ, Tee AR, Cheatham L, Tsou C, Blenis J. mTOR controls cell cycle progression through its cell growth effectors S6K1 and 4E-BP1/eukaryotic translation initiation factor 4E. *Mol Cell Biol*. 2004;24(1):200–216. doi:10.1128/MCB.24.1.200-216.2004

39. Kremer CL, Klein RR, Mendelson J, et al. Expression of mTOR signaling pathway markers in prostate cancer progression. *Prostate*. 2006;66(11):1203–1212. doi:10.1002/pros.20410

40. Balakumaran BS, Porrello A, Hsu DS, et al. MYC activity mitigates response to rapamycin in prostate cancer through eukaryotic initiation factor 4E–binding protein 1–mediated inhibition of autophagy. *Cancer Res*. 2009;69(19):7803–7810. doi:10.1158/0008-5472.CAN-09-0910

41. Graff JR, Konicek BW, Lynch RL, et al. eIF4E activation is commonly elevated in advanced human prostate cancers and significantly related to reduced patient survival. *Cancer Res*. 2009;69(9):3866–3873. doi:10.1158/0008-5472.CAN-08-3472